The Controllable Ball Joint Mechanism*

Yung Cheng TUNG**, Wei-Hua CHIENG** and ShrWai HO***

A controllable ball joint mechanism with three rotational degrees of freedom is proposed in this paper. The mechanism is composed of three bevel gears, one of which rotates with respect to a fixed frame and the others rotate with respect to individual floating frames. The output is the resultant motion of the differential motions by the motors that rotates the bevel gears at the fixed frame and the floating frames. The mechanism is capable of a large rotation, and the structure is potentially compact. The necessary inverse and forward kinematic analyses as well as the derivation of kinematic singularity are provided according to the kinematical equivalent structure described in this paper.

Key Words: Bevel-Gear Mechanisms, Universal Joint, Motion Simulator

1. Introduction

Bevel-gear mechanisms have been shown to have the following advantages: (1) existing closed form solution for inverse kinematics, (2) workspace is easy to be determined, (3) the actuators can be mounted remotely from the center. During past two decades, several studies have been done on these bevel-gear type mechanisms. Chang and Tsai (1989)[1] proposed the first systematic procedure for structural synthesis of spherical mechanisms. The two-DOF geared kinematic chains were generated, and then a ground link was added in series with the input links coaxially to form a three-DOF planetary gear train. Belfiore and Tsai (1991)[2] introduced the concept to develop a new methodology for structural synthesis of three and four-DOF gear train mechanisms. This methodology is based on the partial separation between the kinematic structure and function in order to reduce the dimension of the problem and make any combinational algorithm easy to implement. The graph representation presented by Buchshaum and Freudenstein (1970)[3] often suffers from the problem of pseudo isomorphic graphs (Lin and Tsai, 1989[4]; Freudenstein, 1971[5]).

The analysis of bevel-gear mechanisms is relatively complex, due to the fact that the carriers and planet gears may possess simultaneous angular velocities about non-parallel axes. The conventional tabular or analytical method, which concentrates on planar epicyclic gear trains, is no longer applicable. To overcome this difficulty, Yang and Freudenstein (1973)[6] applied the dual relative velocity and dual matrix of transformation for the analysis of epicyclic bevel-gear trains and hypoid gears. Freudenstein et al. (1984)[7] suggested using the conventional method in conjunction with the Rodrigues equation. Hsu and Lam (1992)[8] has shown an efficient method for developing three-DOF bevel-gear mechanisms synthesized from geared kinematic chains.

This paper presents an innovative mechanism called the controllable ball joint mechanism which is design for the use of a three-DOF motion simulator. This mechanism mainly integrates the universal joint with the differential bevel gear mechanism. The universal joint is located at the center of the mechanism which minimizes the space requirement of the motion simulator. The controllable ball joint mechanism employs coaxial input axles, which requires no complex electrical connector such as rotary joints for the electrical wiring. The key feature for this mechanism is that it employs a simple structure, however, with the capability of high payload.

2. Nomenclatures

O : center point of universal joint
$\boldsymbol{i}$, $\boldsymbol{j}$, $\boldsymbol{k}$: three unit vectors of universal joint that passes through point O
θ_1, θ_2, θ_3 : input angles driven by motors 1, 2, and 3 respectively
$\boldsymbol{j}_4$: unit vectors along axis 4
β_4 : rotation angle along axis 4 relative to j
θ_5 : rotation angle along axis 4 relative to k_5
$\boldsymbol{k}_5$: unit vectors along axis 5
β_6 : rotation angle along axis 4 relative to j_4

* Received 13th January, 2006 (No. 05-5140)
** Department of Mechanical Engineering, National Chiao-Tung University, 1001 Ta Hsueh Road, Hsin-Chu, Taiwan 30010, R.O.C.
*** Department of Automation Engineering, Ta-Hua Institute of Technology, No.1 Dahua Road, Qionglin Shiang, Hsin-Chu, Taiwan 307, R.O.C.

A_1, A_2, A_3, A_4 : pivots of universal revolute joints which points toward O
C_2 : loci of pivots A_2
C_3 : loci of pivots A_3
$\boldsymbol{u}_1$: normalized vector along pivot A_2
$\boldsymbol{v}_4$: normalized vector along pivot A_3
$\boldsymbol{b}$: unit vector perpendiculars to both the input axis and the output axis
$\boldsymbol{b}'$: unit vector perpendiculars to both axis $\boldsymbol{b}$ and $\boldsymbol{w}_{4o}$
$\boldsymbol{u}_1$-$\boldsymbol{v}_1$-$\boldsymbol{w}_1$: coordinate frame which is rotated about axis $\boldsymbol{w}_{1o}$ (= $\boldsymbol{w}_1$) by an angle of ϕ_1 from coordinate frame $\boldsymbol{u}_{1o}$-$\boldsymbol{v}_{1o}$-$\boldsymbol{w}_{1o}$
$\boldsymbol{u}_4$-$\boldsymbol{v}_4$-$\boldsymbol{w}_4$: coordinate frame which is rotated about axis $\boldsymbol{w}_{4o}$ (= $\boldsymbol{w}_4$) by an angle of ϕ_2 from coordinate frame $\boldsymbol{u}_{4o}$-$\boldsymbol{v}_{4o}$-$\boldsymbol{w}_{4o}$
φ : misalign angle of the universal joint
α_1 : intersection angle between axis $\boldsymbol{b}$ and axis $\boldsymbol{u}_1$
α_2 : intersection angle between axis $\boldsymbol{b}'$ and axis $\boldsymbol{v}_4$
ϕ_1 : intersection angle between $\boldsymbol{u}_1$ and $\boldsymbol{u}_{1o}$
ϕ_2 : intersection angle between $\boldsymbol{v}_4$ and $\boldsymbol{v}_{4o}$
G_1, G_2 : Gear contact point (mesh point)

3. Kinematic Structure

The controllable ball joint mechanism consists of seven links, six turning pairs, one universal joint, and two bevel gear pairs. There are three independent axes of rotation. The three axes of rotation intersect at the center point O. The end effector is connected to one of the input links through a universal joint.

The inputs are θ_1, θ_2, θ_3 at link 1, 2, and 3 respectively. Link 2 rotates with respect to link 1 about the $\boldsymbol{k}_1$-axis. The pitch motion is accomplished by rotating link 3 with respect to link 2 about the $\boldsymbol{j}_4$-axis. The roll motion is obtained by rotating axis 4 with respect to link 3 about the $\boldsymbol{k}_5$-axis. Therefore, continuously unobstructed rotations about the three joint axes can be achieved. Figure 1 shows the schematic diagram of the ball joint mechanism.

Figure 2 shows the graph representation of controllable ball joint mechanism. It is composed of nodes, which represent joints, and edges, which represent links. To distinguish the differences between pair connections, gear pairs are denoted by dotted lines, turning pairs (revolute joints) are denoted by simple lines, and the simple lines are labeled according to their axis locations in space. The vertex denoting the fixed link is labeled by two small concentric circles. The links and corresponding vertices are numbered from 0 to 6. The two gear pairs are 3-4 and 4-5. The turning pairs are 0-1, 1-2, 1-3, 2-4, 4-6, and 5-6. The universal joint is inserted between 1 and 5.

The number of degrees of freedom of a mechanism is the minimum number of coordinates necessary to describe its configuration and motion. The number of degrees of freedom of a mechanism, for instance F, may be determined by the Gruebler's mobility equation:

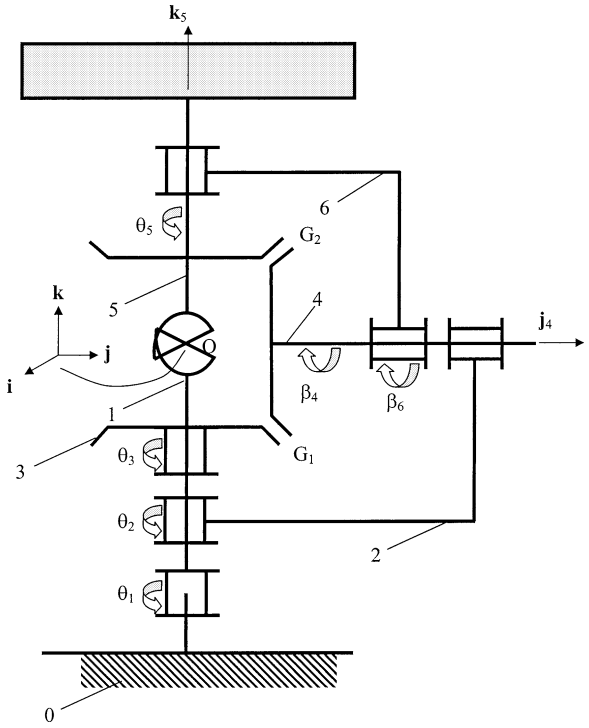

Fig. 1 Schematic diagram of the controllable ball joint mechanism

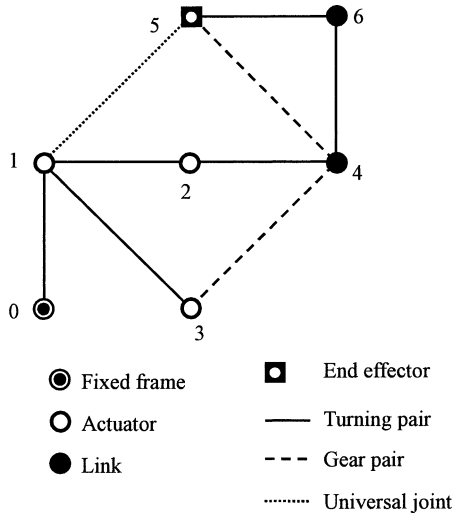

Fig. 2 Graph representation

$$F = \lambda(l - j - 1) + \sum f_j \tag{1}$$

The controllable ball joint mechanism in Fig. 2 consists of seven links, six turning pairs, a universal joint, and two bevel gear pairs. Substituting $l = 7$, $j = 9$, $\sum f_j = 12$, and $\lambda = 3$ which describes the spherical mechanism, Eq. (1) yields that $F = 3$. Therefore, the controllable ball joint mechanism is a three-degree-of-freedom spherical mechanism.

4. Hybrid of Serial-Link and Parallel Manipulators

The serial-link manipulator, such as industrial robots, is used commonly in the automation industry when the

parallel manipulator, such as Steward Platform, is often applied in the motion simulator applications which require the high payload. Differing from the serial-link manipulator the controllable ball joint mechanism employs two transmission paths, one through the bevel gear pairs and the other through the universal joint, from the input link to the output end effector. On the other hand, the controllable ball joint mechanism isn't a fully parallel manipulator which typically consists of extensible legs in a number that equals to the number of degrees of freedom of the mechanism. The controllable ball joint mechanism is a hybrid of serial-link and parallel manipulators, which may be structurally stronger than the serial-link manipulator however weaker than a fully parallel manipulator. The fully parallel manipulator utilizes plural arms, which may interfere one another, to support the end effector, hence it trades off the dexterity and the workspace capacity with its high payload. The controllable ball joint mechanism embodies the merit of good dexterity and workspace capacity from the serial-link manipulator and also the merit of high payload from a parallel manipulator. The application of the controllable ball joint mechanism on the motion simulation to present better motion cues may be sound.

5. Universal Joint

The controllable ball joint mechanism introduced a universal joint between the fixed frame and the end effector. The shaft misalignment angle between the input and output axes of the universal joint is induced by the differential motion of the bevel gears. A general universal joint diagram as shown in Fig. 3 is described by a spherical four bar linkage. Four revolute joints located at position A_1, A_2, A_3, and A_4. Joint axes of these revolute joints are pointing toward the center of the sphere S. Three chords A_1A_2, A_2A_3, A_3A_4 are then always lying on the surface of the sphere. The loci of pivots A_2 and A_3 forms circular contours C_2 and C_3. The practical design of universal joint usually employs the redundancy, which replaces chord A_2A_3 be a cross-pin structure. The coordinate frame $\boldsymbol{u}_{1o}$-$\boldsymbol{v}_{1o}$-$\boldsymbol{w}_{1o}$ is rotated to coordinate frame $\boldsymbol{u}_1$-$\boldsymbol{v}_1$-$\boldsymbol{w}_1$ about axis $\boldsymbol{w}_{1o}$ ($=\boldsymbol{w}_1$) by an angle of ϕ_1, where $\boldsymbol{u}_1$ is the normalized vector of $\overrightarrow{OA_2}$. The rotation transformation matrix is a 3 by 3 matrix and defined that

$$ {}^{1o}_{1}\boldsymbol{R} = R(\boldsymbol{w}_{1o}, \phi_1) \tag{2} $$

The rotational matrix of equivalent axis is

$$ R(\boldsymbol{w}, \phi) = \begin{bmatrix} w_x w_x v\phi + c\phi & w_x w_y v\phi - w_z s\phi & w_x w_z v\phi + w_y s\phi \\ w_x w_y v\phi + w_z s\phi & w_y w_y v\phi + c\phi & w_y w_z v\phi - w_x s\phi \\ w_x w_z v\phi - w_y s\phi & w_y w_z v\phi + w_x s\phi & w_z w_z v\phi + c\phi \end{bmatrix} $$

where $c\phi = \cos\phi$, $s\phi = \sin\phi$, and $v\phi = 1 - \cos\phi$.

The misalign angle between the input axis and the output axis is given as φ about the common axis $\boldsymbol{b}$ of the two circular contours C_2 and C_3. The rotational transformation from the coordinate frame $\boldsymbol{u}_{1o}$-$\boldsymbol{v}_{1o}$-$\boldsymbol{w}_{1o}$ to the coordinate frame $\boldsymbol{u}_{4o}$-$\boldsymbol{v}_{4o}$-$\boldsymbol{w}_{4o}$ is derived as

$$ {}^{1o}_{4o}\boldsymbol{R} = R(\boldsymbol{b}, \varphi) \tag{3} $$

The coordinate frame $\boldsymbol{u}_{4o}$-$\boldsymbol{v}_{4o}$-$\boldsymbol{w}_{4o}$ is rotated to coordinate frame $\boldsymbol{u}_4$-$\boldsymbol{v}_4$-$\boldsymbol{w}_4$ about axis $\boldsymbol{w}_{4o}$ ($=\boldsymbol{w}_4$) by an angle of ϕ_2, where $\boldsymbol{v}_4$ is the normalized vector of vector $\overrightarrow{OA_3}$. The rotational transformation may be written as follows:

$$ {}^{4o}_{4}\boldsymbol{R} = R(\boldsymbol{w}_{4o}, \phi_2) \tag{4} $$

The intersection angle between axis $\boldsymbol{b}$ and axis $\boldsymbol{u}_1$ is denoted as α_1. The unit vector $\boldsymbol{b}'$ as shown in Fig. 3 is perpendicular to both axis $\boldsymbol{b}$ and $\boldsymbol{w}_{4o}$. It is obtained that

$$ \boldsymbol{b}' = \boldsymbol{w}_{4o} \times \boldsymbol{b} $$

The relation of input/output angle of the universal joint is known (Fischer and Freudenstein, 1984[7]) as

$$ \alpha_2 = \tan^{-1}\left(\frac{\tan\alpha_1}{\cos\varphi}\right) \tag{5} $$

The intersection angle α_1 is

$$ \alpha_1 = \tan^{-1}\left(\frac{(\boldsymbol{b}\times\boldsymbol{u}_1)\cdot\boldsymbol{w}_{4o}}{\boldsymbol{b}\cdot\boldsymbol{u}_1}\right) \tag{6} $$

where

$$ \boldsymbol{u}_1 = R(\boldsymbol{w}_{1o}, \phi_1)\boldsymbol{u}_{1o} $$

The intersection angle between $\boldsymbol{v}_4$ and $\boldsymbol{v}_{4o}$ may be obtained that

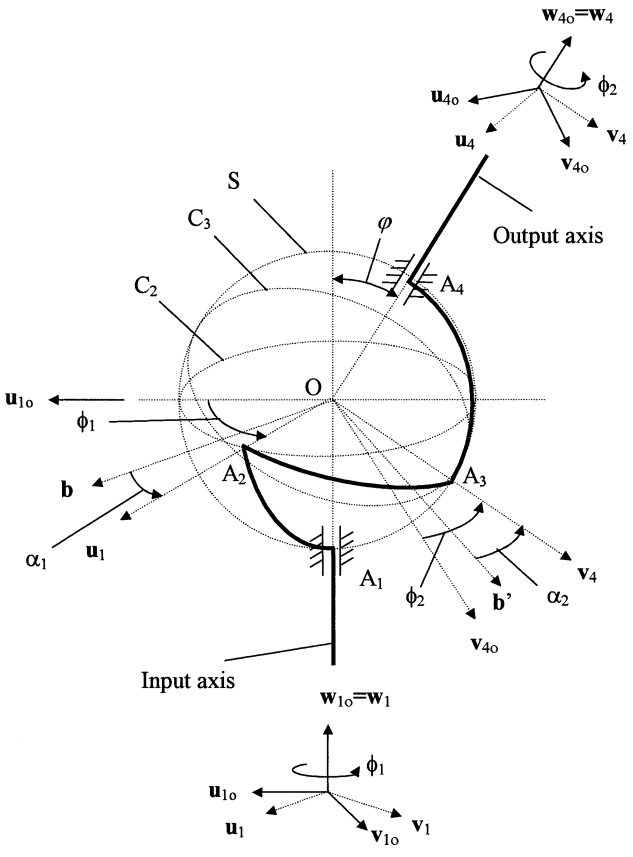

Fig. 3 Coordinate systems in a universal joint

$$\phi_2 = \tan^{-1}\left(\frac{(\boldsymbol{v}_{4o}\times\boldsymbol{b}')\cdot\boldsymbol{w}_{4o}}{\boldsymbol{v}_{4o}\cdot\boldsymbol{b}'}\right)+\alpha_2 \tag{7}$$

The resultant transformation from the coordinate frame $\boldsymbol{u}_{1o}$-$\boldsymbol{v}_{1o}$-$\boldsymbol{w}_{1o}$ to coordinate frame $\boldsymbol{u}_4$-$\boldsymbol{v}_4$-$\boldsymbol{w}_4$ is

$${}^{1o}_{4}\boldsymbol{R} = {}^{1o}_{4o}\boldsymbol{R}\ {}^{4o}_{4}\boldsymbol{R} = R(\boldsymbol{b},\varphi)R(\boldsymbol{w}_{4o},\phi_2)$$

6. Bevel-Gear Mechanism

Kinematic analysis of the ball joint mechanism can be treated as a process to find out the corresponding output orientation from the three input angles. By comparing Fig. 3 with Fig. 1, the following equivalences are found:

$\phi_2 = \theta_5$,

$\varphi = \beta_6$,

$\boldsymbol{w}_{4o} = \boldsymbol{k}_5$,

$\boldsymbol{v}_{4o} = \boldsymbol{j}$,

$\boldsymbol{b} = \boldsymbol{j}_4$, and

$\boldsymbol{u}_1 = \boldsymbol{i}_1$.

This allows the Eq. (7) to be rewritten as follows.

$$\theta_5 = \tan^{-1}\left(\frac{\boldsymbol{j}\times(\boldsymbol{k}_5\times\boldsymbol{j}_4)\cdot\boldsymbol{k}_5}{\boldsymbol{j}\cdot(\boldsymbol{k}_5\times\boldsymbol{j}_4)}\right)+\tan^{-1}\left(\frac{(\boldsymbol{j}_4\times\boldsymbol{i}_1)\cdot\boldsymbol{k}_5}{\boldsymbol{j}_4\cdot\boldsymbol{i}_1\cos\beta_6}\right) \tag{8}$$

According to definition, it is derived that

$$\boldsymbol{i}_1 = R(\boldsymbol{k},\theta_1)\boldsymbol{i}_{1o} = R(\boldsymbol{k},\theta_1)\boldsymbol{i} = [\ \cos\theta_1 \quad \sin\theta_1 \quad 0\ ]^T \tag{9}$$

$$\boldsymbol{j}_4 = R(\boldsymbol{k},\theta_2)\boldsymbol{i}_{4o} = R(\boldsymbol{k},\theta_2)\boldsymbol{j} = [\ -\sin\theta_2 \quad \cos\theta_2 \quad 0\ ]^T \tag{10}$$

$$\boldsymbol{k}_5 = R(\boldsymbol{j}_4,\beta_6)\boldsymbol{k} = [\ \cos\theta_2\sin\beta_6 \quad \sin\theta_2\sin\beta_6 \quad \cos\beta_6\ ]^T \tag{11}$$

thus,

$$\boldsymbol{j}\times(\boldsymbol{k}_5\times\boldsymbol{j}_4)\cdot\boldsymbol{k}_5 = (\boldsymbol{j}\cdot\boldsymbol{j}_4)-(\boldsymbol{j}\cdot\boldsymbol{k}_5)(\boldsymbol{j}_4\cdot\boldsymbol{k}_5) = \cos\theta_2 \tag{12}$$

$$\boldsymbol{j}\cdot(\boldsymbol{k}_5\times\boldsymbol{j}_4) = \sin\theta_2 \tag{13}$$

Substituting Eqs. (9) and (10) into (8), we obtain that

$$\begin{aligned}\theta_5 &= \theta_2 + \tan^{-1}\left(\frac{\tan\theta_2-\tan\theta_1}{1+\tan\theta_2\tan\theta_1}\right)\\ &= \theta_1\end{aligned} \tag{14}$$

Considering the pure rolling condition at the contact point G_1 between two bevel gears indicated as link 4 and link 3, we have the following relation at all instances.

$$\dot{\beta}_4 r_4 + \dot{\theta}_2 r_3 = \dot{\theta}_3 r_3 \tag{15}$$

By assuming that all angles are initially at their zero degree of rotation, Eq. (12) may be further derived as

$$\beta_4 r_4 + \theta_2 r_3 = \theta_3 r_3 \tag{16}$$

Considering the pure rolling condition at the contact point G_2 between two epicyclic gears indicated as link 5 and link 4, we have

$$-\beta_6 r_4 + \theta_5 r_5 = -\beta_4 r_4 + \theta_2 r_3 \tag{17}$$

where r_3, r_4, and r_5 denotes the radius of the gear on link 3, 4, and 5 respectively. From Eq. (16), we obtain that

$$\beta_4 = \frac{(\theta_3-\theta_2)r_3}{r_4} \tag{18}$$

Combining Eqs. (14), (17) and (18), we have

$$\begin{aligned}\beta_6 &= \frac{\theta_5 r_5 - (2\theta_2-\theta_3)r_3}{r_4}\\ &= \frac{\theta_1 r_5 - (2\theta_2-\theta_3)r_3}{r_4}\end{aligned} \tag{19}$$

As shown in Fig. 1, it is necessary to have $r_3 = r_5$ in order to have a proper bevel gear mesh at gear 4. Let $\xi = r_4/r_5$, Eq. (19) yields that

$$\beta_6 = \frac{\theta_3+\theta_1-2\theta_2}{\xi} \tag{20}$$

From Eqs. (14) and (20), it is obtained that

$$\begin{bmatrix}\theta_2\\ \beta_6\\ \theta_5\end{bmatrix} = \frac{1}{\xi}\begin{bmatrix}0 & \xi & 0\\ 1 & -2 & 1\\ \xi & 0 & 0\end{bmatrix}\begin{bmatrix}\theta_1\\ \theta_2\\ \theta_3\end{bmatrix} \tag{21}$$

7. Forward Kinematics of the Controllable Ball Joint Mechanism

According to Fig. 1, the rotational transformation from ground and link 5 can be derived as follows:

$$\begin{aligned}{}^0_5\boldsymbol{T} &= R(\boldsymbol{k},\theta_2)R(\boldsymbol{j}_4,\beta_6)R(\boldsymbol{k}_5,\theta_5-\theta_2)\\ &= \begin{bmatrix}a_{11} & a_{12} & a_{13}\\ a_{21} & a_{22} & a_{23}\\ a_{31} & a_{32} & a_{33}\end{bmatrix}\end{aligned} \tag{22}$$

The entries of matrix ${}^0_5\boldsymbol{T}$ are enumerated and listed in Appendix I. The arguments θ_1, β_6, and $(\theta_5-\theta_2)$, in Eq. (21) are also known as *Z-Y-Z* Euler angles.

The output angle is defined in terms of *X-Y-Z* Euler angles, the transformation is derived by initially rotates about the *X*-axis by a roll angle γ, then rotates about the *Y*-axis by a pitch angle β, and then rotate about the *Z*-axis by a yaw angle α.

$$\begin{aligned}\boldsymbol{R}_{XYZ} &= R(\boldsymbol{k},\alpha)R(\boldsymbol{j},\beta)R(\boldsymbol{i},\gamma)\\ &= \begin{bmatrix}c_{11} & c_{12} & c_{13}\\ c_{21} & c_{22} & c_{23}\\ c_{31} & c_{32} & c_{33}\end{bmatrix}\\ &= {}^0_5\boldsymbol{T}\end{aligned} \tag{23}$$

The entries of matrix $\boldsymbol{R}_{XYZ}$ are enumerated and listed in Appendix II. The following relations are then derived.

$$\begin{aligned}\beta &= \tan^{-1}\left(\frac{-a_{31}}{\sqrt{a_{11}^2+a_{21}^2}}\right)\\ &= \tan^{-1}\left(\frac{\sin\theta_2\cos\beta_6\cos(\theta_1-\theta_2)+\cos\theta_2\sin(\theta_1-\theta_2)}{\cos\theta_2\cos\beta_6\cos(\theta_1-\theta_2)-\sin\theta_2\sin(\theta_1-\theta_2)}\right)\end{aligned} \tag{24}$$

$$\alpha = \tan^{-1}\left(\frac{a_{21}/\cos\beta}{a_{11}/\cos\beta}\right)$$
$$= \tan^{-1}\left(\frac{(\sin\theta_2\cos\beta_6\cos(\theta_1-\theta_2)+\cos\theta_2\sin(\theta_1-\theta_2))/\cos\beta}{(\cos\theta_2\cos\beta_6\cos(\theta_1-\theta_2)-\sin\theta_2\sin(\theta_1-\theta_2))/\cos\beta}\right) \quad (25)$$

$$\gamma = \tan^{-1}\left(\frac{a_{32}/\cos\beta}{a_{33}/\cos\beta}\right)$$
$$= \tan^{-1}\left(\frac{-\sin(\theta_1-\theta_2)\sin((\theta_3+\theta_1-2\theta_2)/\xi)/\cos\beta}{\cos((\theta_3+\theta_1-2\theta_2)/\xi)/\cos\beta}\right) \quad (26)$$

where

$$\beta_6 = \frac{\theta_1-2\theta_2+\theta_3}{\xi}$$

8. Inverse Kinematics of the Controllable Ball Joint Mechanism

For solving the inverse kinematics problem, mapping the Cartesian space to joint space. The *X-Y-Z* fixed angle frame is introduced with angles of roll γ, pitch β, and yaw α.

$$^0_5\boldsymbol{T} = R(\boldsymbol{k},\theta_2)R(\boldsymbol{j}_4,\beta_6)R(\boldsymbol{k}_5,\theta_5-\theta_2) = \boldsymbol{R}_{XYZ} \quad (27)$$

It is derived that

$$\beta_6 = \tan^{-1}\left(\frac{\sqrt{c_{13}^2+c_{23}^2}}{c_{33}}\right) = \xi\tan^{-1}\left(\frac{\sqrt{\sin^2\beta\cos^2\gamma+\sin^2\gamma}}{\cos\beta\cos\gamma}\right) \quad (28)$$

$$\theta_2 = \tan^{-1}\left(\frac{c_{23}/\sin\beta_6}{c_{13}/\sin\beta_6}\right) = \tan^{-1}\left(\frac{(\sin\alpha\sin\beta\cos\gamma-\cos\alpha\sin\gamma)/\sin\beta_6}{(\cos\alpha\sin\beta\cos\gamma+\sin\alpha\sin\gamma)/\sin\beta_6}\right) \quad (29)$$

$$\theta_1 = \tan^{-1}\left(\frac{c_{32}/\sin\beta_6}{c_{31}/\sin\beta_6}\right)+\theta_2 = \tan^{-1}\left(\frac{\cos\beta\sin\gamma/\sin\beta_6}{-\sin\beta/\sin\beta_6}\right)+\theta_2 \quad (30)$$

$$\theta_3 = 2\theta_2-\theta_1+\beta_6 \quad (31)$$

9. Kinematic Singularities

The inverse Jacobian matrix that correlates the outputs, i.e. the Cartesian space angles γ, β, and α, to the inputs, i.e. the joint space angles θ_1, θ_2, and θ_3 may be derived as follows.

$$\begin{bmatrix}\dot\theta_1\\ \dot\theta_2\\ \dot\theta_3\end{bmatrix} = \boldsymbol{J}_q\begin{bmatrix}\dot\alpha\\ \dot\beta\\ \dot\gamma\end{bmatrix} \quad (32)$$

where

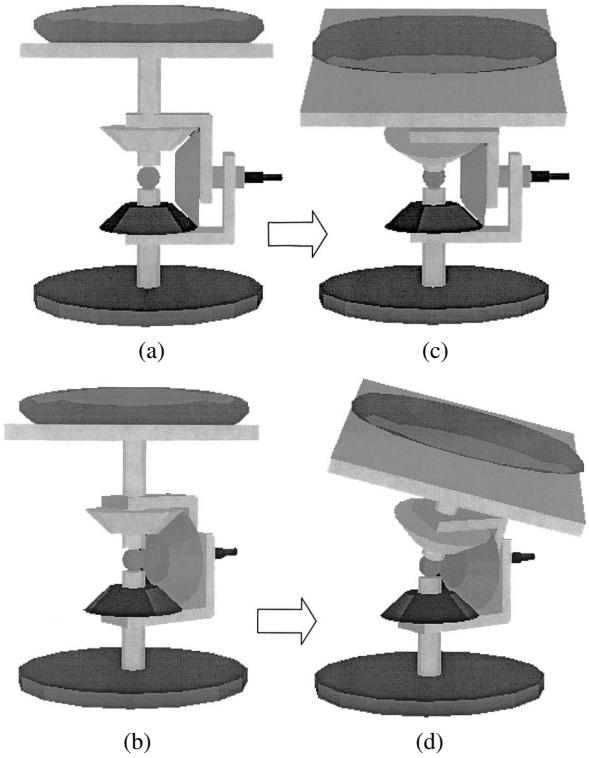

Fig. 4 Kinematic singularity examples

$$\boldsymbol{J}_q = \begin{bmatrix}k_{11} & k_{12} & k_{13}\\ k_{21} & k_{22} & k_{23}\\ k_{31} & k_{32} & k_{33}\end{bmatrix} \quad (33)$$

The entries of the inverse Jacobian matrix obtained from Eqs. (28) to (31) are listed in Appendix III. A kinematic singularity occurs when any entry of $\boldsymbol{J}_q$ goes to infinity. It may be immediately seen from Appendix III that the inverse Jacobian matrix is irrelevant with the yaw angle α. Thus, different angles of yaw α can cause no singularity. Different kinematic singularities may be verified throughout all entries. As an example, it is obtained from Appendix III that the singularity occurs at

$$\sin^2\beta\csc\gamma+\cos^2\beta\sin\gamma = 0,$$

which yields that the singularity occurs at $\beta = \gamma = 0°$ or 180°.

Figure 4 (a) and (c) compares two different postures can possibly obtained due to output Euler angles $\beta = \gamma = 0°$. Starting from the posture in Fig. 4 (a), the end effector can only bend forward to perform the output pitch velocity $\dot\beta$ as shown in Fig. 4 (c). On the other hand, starting from the posture in Fig. 4 (b), the end effector will produce a constrained output roll velocity that $\dot\alpha = \mu\dot\beta$, where μ is a constant depending on the posture, as shown in Fig. 4 (d).

10. Implementation and Result

Figure 5 demonstrates an actual implementation of the controllable ball joint mechanism according to Fig. 1. Three motors are used for driving each of the input links

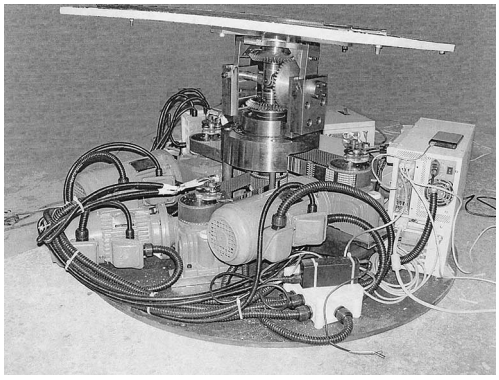

Fig. 5 Photo of the actual implementation

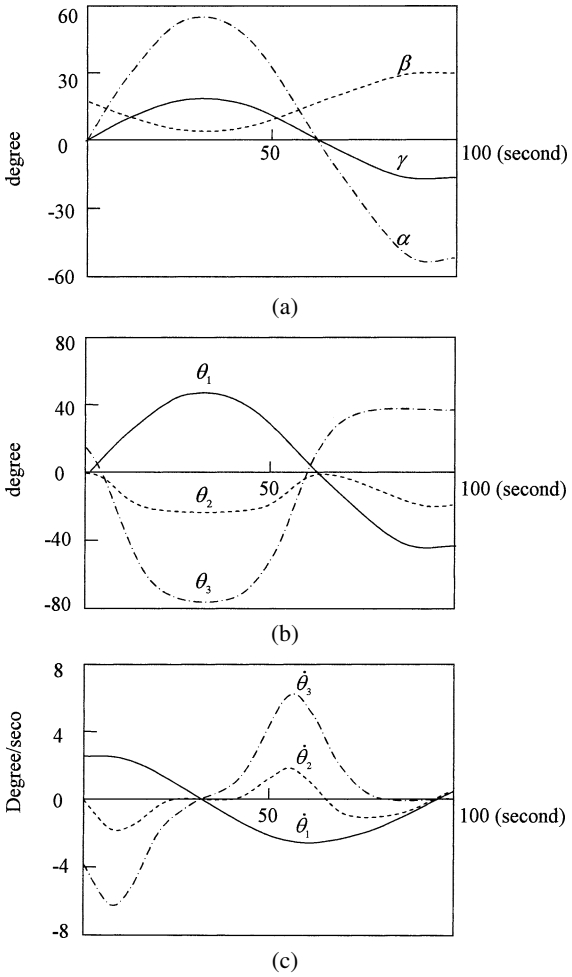

Fig. 6 Inverse kinematics: (a) given output Euler angles, (b) calculated input angle, and (c) calculated input velocity

via belts and pulleys. Subjected to the output Euler angles that $\alpha = \frac{\pi}{10}\cos\omega t$, $\beta = -\frac{\pi}{12}\cos\omega t + \frac{\pi}{50}$ and $\gamma = \frac{3\pi}{10}\cos\omega t$ as shown in Fig. 6 (a), the input link rotation, according to Eqs. (28) to (31), are calculated and shown in Fig. 6 (b) and (c). Note that there is no singularity in the above trajectory for it is confined that $\beta > 0$.

Dexterity associated with the speed limitation of the input can be considered as the ability of the manipulator to arbitrarily drive its pose, or apply wrenches in arbitrary directions. Figure 7 (a) shows the result when the motor speed limitation 3 degree/sec is applied to the speed of the input link in Fig. 6 (c). Comparing the input in Fig. 6 (a) with the forward kinematics result in Fig. 7 (c), it is found that the output yaw angle α is less sensitive to the speed limitation when other Euler angles when other output angles are distorted due to the same speed limitation.

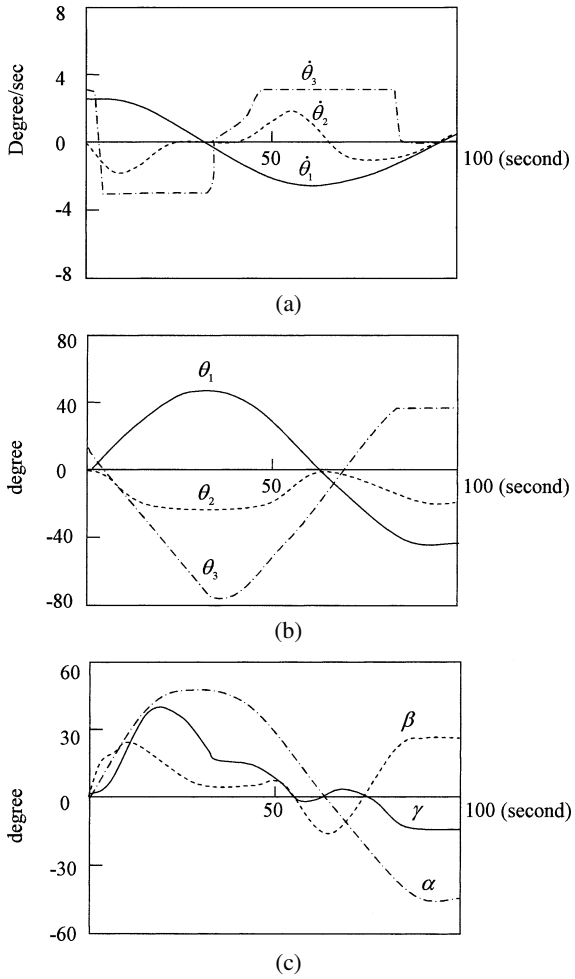

Fig. 7 Forward kinematics: (a) given input velocity, (b) the corresponding input angle, and (c) calculated output Euler angles

11. Experiments

Referring to Fig. 5, the proposed controllable ball joint mechanism employs three AC induction motors. Each motor is coupled to a 1 : 50 gear head. The outputs of the gear heads connected to the individual input axles through timing belts. The specifications of the major components are given as follows.

(a) Motor:
AC induction motor: 220 VAC, 60 Hz
Output power: 3.7 kW
Rated speed: 1 745 RPM

Rated torque: 2.080 kg · m

(b) Motor drive: ATV31HU40M3X, Telemecanique

(c) Gear head ratio: 1 : 50

(d) Timing belt pulley ratio: 1 : 1

(e) Bevel gears' specification:

	Module	Number of Teeth	Pressure Angle	Radius
Gear 3	3	50	20°	$r_3 = 75mm$
Gear 4	3	80	20°	$r_4 = 120mm$
Gear 5	3	50	20°	$r_5 = 75mm$

The pitch and roll workspace of the motion simulator is limited by the maximum misalignment angle of the universal joint. The yaw workspace is ±180°, i.e.

$$\gamma_{\max} = \beta_{\max} = \pm 30^\circ$$

$$\alpha_{\max} = \pm 180^\circ$$

The digital controller mainly consists of an industrial PC with Pentium IV CPU. The AD/DA card is used, for a low cost concern, to directly convert the commands from the controller to analog output and feed to the motor drive.

Figure 8 shows the result from the experiments. Figure 8 (a) shows a set of motion instructions recorded from an interactive game. The motion instructions are given in Euler angles as the desired output. These output Euler angles are then fed to the digital controller for calculating the input angle command according to Eqs. (28) to (31). The input angle command of each input axle, as shown in Fig. 8 (b), is converted to the analog voltage command and fed to the motor drive. The actual input angle of each input axle is obtained by recording the encoder positions, which is shown in Fig. 8 (c). The difference between the input angle command and actual input angle is resulted from the servo response including the gain and phase corresponding to different frequencies. Due to the presence of the servo response, the actual Euler angle output, as shown in Fig. 8 (d), is different from the desired Euler angle as shown in Fig. 8 (a). The servo response determines the trajectory following error of the output Euler angles of the motion simulator. Adjustment of the servo response must follow the optimization of certain motion performance index which is beyond the topic of this paper. In fact, the proposed mechanism is verified useful to be a motion simulator.

12. Conclusion

An innovative design of three degrees-of-freedom mechanism, called controllable ball joint mechanism, combining the conventional robot wrist and a universal joint is presented in this paper. Closed-form solutions for the inverse and forward kinematics of this mechanism are also derived. According to the kinematic singularity analysis, it is found that the mechanism is singular at its neutral position of roll and pitch angles. Hence either the

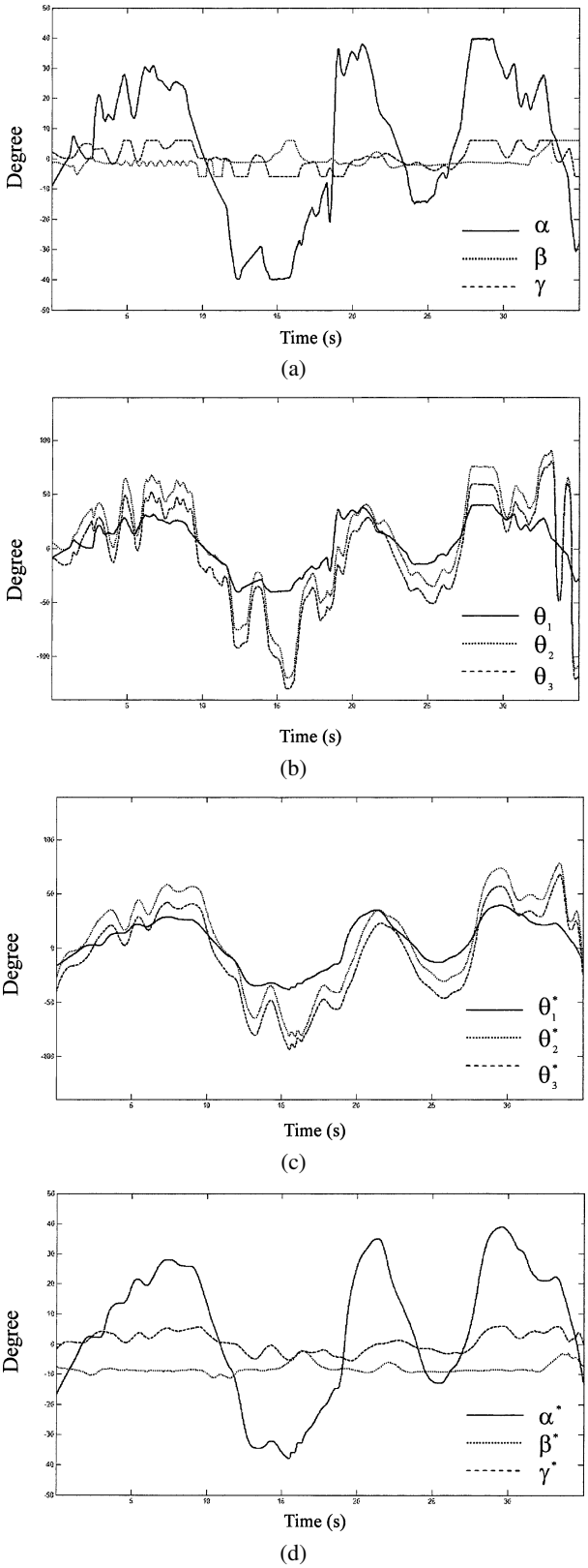

Fig. 8 Experimental data: (a) given output Euler angles of the upper platform, (b) input angle of each input axle calculated by controller, (c) actual input angle of each input axle read from encoders, and (d) actual output Euler angles derived from the actual input angles

roll or the pitch angle of this mechanism must be confined away from zero in order to avoid the kinematic singularity. Such mechanism is potentially useful to the applications of three degrees-of-freedom motion simulator. It can be implemented, with a real-time controller, as a personal entertainment platform or vehicle simulator to disorient the pilot or passenger into an exciting virtual world.

Acknowledgements

This research was supported by the R.O.C. National Science Council under contract No. NSC93-2218-E-009-013.

Appendix I

Entries of matrix ${}^0_5\boldsymbol{T}$

$$a_{11}=\cos\theta_2\cos\beta_6\cos(\theta_5-\theta_2)-\sin\theta_2\sin(\theta_5-\theta_2)$$
$$a_{12}=-\cos\theta_2\cos\beta_6\sin(\theta_5-\theta_2)-\sin\theta_2\cos(\theta_5-\theta_2)$$
$$a_{13}=\cos\theta_2\sin\beta_6$$
$$a_{21}=\sin\theta_2\cos\beta_6\cos(\theta_5-\theta_2)+\cos\theta_2\sin(\theta_5-\theta_2)$$
$$a_{22}=-\sin\theta_2\cos\beta_6\sin(\theta_5-\theta_2)+\cos\theta_2\cos(\theta_5-\theta_2)$$
$$a_{23}=\sin\theta_2\sin\beta_6$$
$$a_{31}=-\sin\beta_6\cos(\theta_5-\theta_2)$$
$$a_{32}=-\sin\beta_6\sin(\theta_5-\theta_2)$$
$$a_{33}=\cos\beta_6$$

Appendix II

Entries of matrix $\boldsymbol{R}_{XYZ}$

$$c_{11}=\cos\alpha\cos\beta$$
$$c_{12}=\cos\alpha\sin\beta\sin\gamma-\sin\alpha\cos\gamma$$
$$c_{13}=\cos\alpha\sin\beta\cos\gamma+\sin\alpha\sin\gamma$$
$$c_{21}=\sin\alpha\cos\beta$$
$$c_{22}=\sin\alpha\sin\beta\sin\gamma+\cos\alpha\cos\gamma$$
$$c_{23}=\sin\alpha\sin\beta\cos\gamma-\cos\alpha\sin\gamma$$
$$c_{31}=-\sin\beta$$
$$c_{32}=\cos\beta\sin\gamma$$
$$c_{33}=\cos\beta\cos\gamma$$

Appendix III

Entries of the Jacobian matrix in Eq. (33)

$$k_{11}=\frac{\partial\theta_1}{\partial\alpha}=-1$$
$$k_{12}=\frac{\partial\theta_1}{\partial\beta}$$
$$=\frac{1}{\sin^2\beta\csc\gamma+\cos^2\beta\sin\gamma}+\frac{1}{\cos\beta\cot\gamma-\sec\beta\csc\gamma\sec\gamma}$$
$$k_{13}=\frac{\partial\theta_1}{\partial\gamma}$$
$$=-\frac{1}{\tan\beta\sec\gamma+\cot\beta\sin\gamma\tan\gamma}+\frac{1}{\sin\beta\cos^2\gamma+\csc\beta\sin^2\gamma}$$
$$k_{21}=\frac{\partial\theta_2}{\partial\alpha}=-1$$
$$k_{22}=\frac{\partial\theta_2}{\partial\beta}=\frac{1}{\cos\beta\cot\gamma-\sec\beta\csc\gamma\sec\gamma}$$
$$k_{23}=\frac{\partial\theta_2}{\partial\gamma}=\frac{1}{\sin\beta\cos^2\gamma+\csc\beta\sin^2\gamma}$$
$$k_{31}=\frac{\partial\theta_3}{\partial\alpha}=-2$$
$$k_{32}=\frac{\partial\theta_3}{\partial\beta}$$
$$=\frac{1}{\sin^2\beta\csc\gamma+\cos^2\beta\sin\gamma}-\frac{\xi\sin\beta\cos\gamma}{\sqrt{\sin^2\beta+\cos^2\beta\sin^2\gamma}}$$
$$-\frac{2}{\cot\gamma\sin\beta\tan\beta+\sec\beta\tan\gamma}$$
$$k_{33}=\frac{\partial\theta_3}{\partial\gamma}$$
$$=\frac{4\left[(\cos\beta\cos\gamma-2)\sin\beta+\xi\cos\beta\cos\gamma\sqrt{\sin^2\beta+\cos^2\beta\sin^2\gamma}\right]}{\cos(2\beta)+2\cos^2\beta\cos(2\gamma)-3}$$

References

(1) Chang, S.L. and Tsai, L.W., Topological Synthesis of Articulated Gear Mechanisms, IEEE J. Robot. Autom., Vol.6, No.1 (1989), pp.97–103.

(2) Belfiore, N.P. and Tsai, L.W., A New Methodology for Structural Synthesis of Geared Robotic Wrist, Proceedings of the 2nd National Conference on Applied Mechanisms and Robotics, Paper No.VIB-5 (1991), pp.1–7.

(3) Buchsbaum, F. and Freudenstein, F., Synthesis of Kinematic Structure of Geared Kinematic Chains and Other Mechanism, Journal of Mechanism, No.5 (1970), pp.357–392.

(4) Lin, C.C. and Tsai, L.W., The Development of an Atlas of Bevel-Gear-Type Spherical Wrist Mechanism, Proceedings of the First National Conference on Applied Mechanisms and Robotics, Paper No.89AMR-2A-3, (1989).

(5) Freudenstein, F., An Application of Boolean Algebra to the Motion of Epicyclic Drives, ASME Journal of Engineering for Industry, 93B (1971), pp.176–182.

(6) Yang, A.T. and Freudenstein, F., Mechanics of Epicyclic Bevel-Gear Trains, ASME J. Eng. Ind., Ser.B, Vol.95, No.2 (1973), pp.497–502.

(7) Fischer, I.S. and Freudenstein, F., Internal Force and Moment Transmission in a Cardan Joint with Manufacturing Tolerance, ASME J. of Mechanisms, Transmissions, and Automation in Design, (1984), pp.301–311.

(8) Hsu, C.H. and Lam, K.T., A New Graph Representation for the Automatic Kinematic Analysis of Planetary Spur-Gear Trains, ASME Journal of Mechanical Design, 114 (1992), pp.196–200.